An Increase in Voltage-Gated Sodium Channel Current Elicits Microglial Activation Followed Inflammatory Responses *In Vitro* and *In Vivo* After Spinal Cord Injury

Gil Y. Jung,[1] Jee Y. Lee,[1,2] Hyewhon Rhim,[3] Tae H. Oh,[1] and Tae Y. Yune[1,2,4]

Inflammation induced by microglial activation plays a pivotal role in progressive degeneration after traumatic spinal cord injury (SCI). Voltage-gated sodium channels (VGSCs) are also implicated in microglial activation following injury. However, direct evidence that VGSCs are involved in microglial activation after injury has not been demonstrated yet. Here, we show that the increase in VGSC inward current elicited microglial activation followed inflammatory responses, leading to cell death after injury *in vitro* and *in vivo*. Isoforms of sodium channel, $Na_v1.1$, $Na_v1.2$, and $Na_v1.6$ were expressed in primary microglia, and the inward current of VGSC was increased by LPS treatment, which was blocked by a sodium channel blocker, tetrodotoxin (TTX). TTX inhibited LPS-induced NF-κB activation, expression of TNF-α, IL-1β and inducible nitric oxide synthase, and NO production. LPS-induced p38MAPK activation followed pro-nerve growth factor (proNGF) production was inhibited by TTX, whereas LPS-induced JNK activation was not. TTX also inhibited caspase-3 activation and cell death of primary cortical neurons in neuron/microglia co-cultures by inhibiting LPS-induced microglia activation. Furthermore, TTX attenuated caspase-3 activation and oligodendrocyte cell death at 5 d after SCI by inhibiting microglia activation and p38MAPK activation followed proNGF production, which is known to mediate oligodendrocyte cell death. Our study thus suggests that the increase in inward current of VGSC appears to be an early event required for microglia activation after injury.

GLIA 2013;61:1807–1821

Key words: microglia; spinal cord injury; tetrodotoxin; voltage-gated sodium channels

Introduction

Inflammation has been known as one of major processes during the neurodegenerative pathogenesis after spinal cord injury (SCI) (Beattie et al., 2002; Chan, 2008; Donnelly and Popovich, 2008). Microglia, the endogenous immune cells in the CNS, are rapidly activated in response to injuries including SCI and known to play as a sensor for pathological events in the CNS (David and Kroner, 2011; Hanisch and Kettenmann, 2007; Kreutzberg, 1996). Activated microglia lead to various functions such as proliferation, migration, phagocytosis, and secretion of multiple cytokine/chemokines, which are mediated by a complex process involving multiple signaling cascades (Colton, 2009; David and Kroner, 2011; Hanisch and Kettenmann, 2007; Ransohoff and Perry, 2009). Furthermore, microglia are known to contribute to neurodegenerative processes after SCI by releasing inflammatory cytokines and mediators such as tumor necrosis factor (TNF)-α, interleukin (IL)-1β, and nitric oxide (NO), leading to apoptotic cell death and ultimately functional impairment (Beattie, 2004; Tian et al., 2007; Xu et al., 2007; Yune et al., 2003).

Microglia express a wide variety of ion channels including K^+, H^+, Cl^-, and Ca^{2+} channels, which are known to maintain the membrane potential and mediate microglial functions such as proliferation, migration and ramification and de-ramification (Eder, 1998, 2005; Farber and Kettenmann, 2005; Illes et al., 1996). Microglia are also known to express voltage-gated sodium channels (VGSC) which are demonstrated by electrophysiological techniques in rodent

View this article online at wileyonlinelibrary.com. DOI: 10.1002/glia.22559

Published online August 30, 2013 in Wiley Online Library (wileyonlinelibrary.com). Received Jan 8, 2013, Accepted for publication July 12, 2013.

Address correspondence to Tae Y. Yune, Department of Biochemistry and Molecular Biology, School of Medicine, Kyung Hee University, Medical Building 10th Floor, Dongdaemun-gu, Hoegi-dong 1, Seoul 130-701, Korea. E-mail: tyune@khu.ac.kr

From the [1]Age-Related and Brain Diseases Research Center, School of Medicine, Kyung Hee University, Seoul, Korea; [2]Neurodegeneration Control Research Center, School of Medicine, Kyung Hee University, Seoul, Korea; [3]Center for Neuroscience, Korea Institute of Science & Technology, Seoul, Korea; [4]Department of Biochemistry and Molecular Biology, School of Medicine, Kyung Hee University, Seoul, Korea.

and human microglia (Korotzer and Cotman, 1992; Norenberg et al., 1994). In addition, sodium channels are implicated in microglia/macrophage activation and function in experimental autoimmune encephalomyelitis and multiple sclerosis (Craner et al., 2005) by showing that sodium channel activity modulates multiple functions such as phagocytosis, cytokine release and migration in microglia (Black et al., 2009; Black and Waxman, 2012). Therefore, it can be postulated that VGSC in microglia can be one of initial events required for microglial activation after injury. However, the direct physiological and molecular evidences for the involvement of VGSC in microglial activation have not been demonstrated yet.

In this study, we tested a hypothesis that the increase in VGSC current may be involved in microglial activation after injury. We found that its inward current was increased in primary microglia by lipopolysaccharide (LPS) treatment, which was completely blocked by sodium channel blocker, tetrodotoxin (TTX). TTX also inhibited inflammatory responses in microglia. In addition, the upregulation of sodium channels by LPS was required for microglial activation. Furthermore, TTX inhibited LPS-induced neuronal cell death in primary cortical neurons co-cultured with microglia and oligodendrocyte cell death after SCI.

Materials and Methods

Primary Cultures

Rat primary neurons were isolated from the cerebral cortices of embryonic 17 d Sprague-Dawley rats (SD, Samtako, Osan, Korea) according to the protocol described previously (Lee et al., 2004). Briefly, cerebral cortices removed with meninges were dissected in HBSS solution (Invitrogen, Carlsbad, CA) and were dissociated by trypsinization followed by triturating and passed through a 210-μm nylon mesh (Invitrogen). Cells (1×10^5 cells) were seeded on poly-D-lysine (20 μg/mL, Sigma, St. Louis, MO)-coated 24-well plates or 12 mm glass coverslips, and maintained in neurobasal media (Invitrogen) supplemented with B27 (Invitrogen) and 0.5 mM glutamine in a humidified 5% CO_2 incubator at 37°C. Culture medium was replaced with fresh medium every 2 d for 1 week and cells were then used. Immunocytochemistry using an antibody specific for neurons (NeuN, 1:100; Chemicon) revealed that the purity of neuronal population was greater than 95%. Enriched primary microglia cultures were derived from mixed glial cultures. The mixed glial cells were prepared from SD rat brains on postnatal day 1-2 according to the protocol described above. The mixed glial cells were seeded at a density of 1×10^7 cells per 75 cm^2 flask and cultured in DMEM supplemented with 5% fetal bovine serum (FBS) and 100 units/mL penicillin and 100 μg/mL streptomycin at 37°C in a humidified incubator under 5% CO_2. After 8 d, the flasks were shaken at 200 r.p.m. at 37°C for 1 h. Floating cells were harvested and seeded onto poly-D-lysine-coated 6-well plate at a density of 8×10^5 cells in DMEM (Invitrogen) supplemented with 10% FBS. By immunocytochemical analysis, more than 98% of the cells were stained positively for a microglial marker (OX-42 antibody, 1:100; Millipore, Billerica, MA). For neuron/microglia co-cultures, microglia (1×10^5 cells per well) were grown on porous upper inserts of Transwell chambers (3-μm diameter pores, BD Biosciences, San Jose, CA) in 24-well plates. After treatment with LPS (1 μg/mL, Millipore) for 1 h, with or without TTX (1 μM), the inserts were washed and placed above cortical neurons growing on a coverslip in the bottom well of the Transwell chambers, allowing diffusion of soluble molecules. Under this culture condition, neurons were never exposed to LPS or TTX.

Abbreviations

COX-2	Cyclooxygenase-2
IL-1β	interleukin-1β
JNK	c-Jun N-terminal kinases
LDH	Lactate dehydrogenase
LPS	Lipopolysaccharide
NF-κB	Nuclear factor kappa-B
NGF	Nerve growth factor
NO	Nitric oxide
p38MAPK	p38 mitogen activated protein kinase
SCI	Spinal cord injury
TUNEL	Terminal deoxynucleotidyl transferase-mediated deoxyuridine triphosphate-biotin nick end labeling
TNF-α	Tumor necrosis factor
TLR-4	Toll-like receptor 4
TTX	Tetrodotoxin
VGSC	Voltage-gated sodium channels

Electrophysiology

Electrophysiological recordings from primary microglia were carried out using the perforated whole-cell patch-clamp technique at room temperature. Borosilicate glass electrodes with resistance of 3–5 MΩ were pulled. For the recording of inward currents of VGSC, the composition of the internal and external solution is followed as: internal solution, 144 mM KGlu, 2 mM $MgCl_2$, 0.5 mM EGTA, 10 mM 4-(2-hydroxyethyl)-1-piperazineethanesulfonic acid (HEPES) and 4 mM Mg-ATP (pH 7.2) and external solution, 120 mM NaCl, 4.5 mM KCl, 2 mM $MgCl_2$, 22 mM $NaHCO_3$, 1 mM $CaCl_2$, 10 mM glucose, and 10 mM HEPES (pH 7.2). Standard current-voltages (I-V) were obtained using 50 ms pulses from a holding potential of −80 mV, to a range of potentials (−60 to 90 mV) every 10 s. Currents were filtered at 10 kHz and sampled at 100 kHz. Current recordings were obtained with an EPC-9 amplifier and Pulse/Pulsefit software (HEKA, Germany). The series resistance was compensated up to 75–90%. For current density measurements, the currents were divided by the cell capacitance, as read from the amplifier. Data are expressed as mean ± SEM, and statistical analyses were performed using the Student's *t*-test.

Assessment of Cytotoxicity

Cell cytotoxicity was assessed using the lactate dehydrogenase (LDH) assay kit (Sigma) according to the manufacturer's instructions. Absorbance data were obtained using a microplate reader (Spectra Max 340; Molecular Devices, Sunnyvale, CA) with a 450 nm filter, and 650 nm as reference wavelength. Maximum LDH release was determined by cell lysis of one well of untreated cells by cell culture

media containing LDH assay lysis solution. Values were expressed relative to measurement from maximal LDH.

Measurement of Nitric Oxide

After LPS (1 μg/mL) treatment, NO production was measured as nitrite accumulated in the culture medium after 24 h. One hundred microliter of culture supernatant was reacted with an equal volume of Griess reagent (Sigma) and incubated at 37°C for 30 min. Absorbance was measured at 540 nm with a microplate reader (Molecular devices). Activity was expressed in terms of the nitrite concentration as determined from a standard sodium nitrite curve.

Spinal Cord Injury

Male SD rats (250–300 g) were anesthetized with chloral hydrate (500 mg/kg, i.p.) and a laminectomy was performed at the T9-T10 level exposing the cord beneath without disrupting the dura. The spinous processes of T8 and T11 were then clamped to stabilize the spine, and the exposed dorsal surface of the cord was subjected to a moderate contusion injury (10 g × 25 mm) using a NYU impactor as previously described (Yune et al., 2007). For the sham-operated controls, the animals underwent a T10 laminectomy without weight-drop injury. All surgical interventions and postoperative animal care were performed in accordance with the Guidelines and Polices for Rodent Survival Surgery provided by the Animal Care Committee of the Kyung Hee University.

Microinjection of TTX

TTX administration was performed according to the previous reported method (Teng and Wrathall, 1997) with a minor modification. Briefly, TTX was dissolved in PBS at a final concentration of 100 μM, and 2 μL of TTX (0.15 nmole) was administered into the lesion epicenter using a glass micropipette attached to a 5 μL Hamilton syringe connected to a micromanipulator (David Kopf Instruments, Tujunga, CA). Drug administration was performed at a depth of 1 mm below the cord surface at a 0.3 μL/min of delivery rate.

Tissue Preparation

At 5 d after SCI, animals were anesthetized with chloral hydrate (500 mg/kg, i.p.) and perfused via cardiac puncture initially with 0.1 M PBS (pH 7.4) and subsequently with 4% paraformaldehyde in 0.1 M phosphate buffer (PB). A 20-mm section of the spinal cord, centered at the lesion site, was dissected out, post-fixed by immersion in the same fixative for 6 h and placed in 30% sucrose in 0.1 M PBS. The segment was embedded in OCT for frozen sections as described previously (Yune et al., 2007). Frozen tissue sections were then cut at 10 μm on a cryostat (CM1850; Leica, Germany). For molecular and biochemical works, animals were perfused with 0.1 M PBS and segments of spinal cord (10 mm) including the lesion site were isolated and frozen at −80°C.

RNA Isolation and RT-PCR

RNA isolation from primary microglia using TRIZOL Reagent (Invitrogen) and cDNA synthesis were performed as previously described (Yune et al., 2007). A 20 μL PCR reaction contained 1 μL first strand cDNA, 0.5 U taq polymerase (Takara, Kyoto, Japan), 20 mM Tris-HCl, pH 7.9, 100 mM KCl, 1.5 mM $MgCl_2$, 250 μM dNTP, and 10 pmole of each specific primer. Samples were subjected to 25–30 cycles of 95 C 30 s, 50–62 C 30 s, and 72 C for 30 s on a thermocycler (Takara). The primers used for this experiment were designed according to the sequences previously reported for $Na_v1.1$, $Na_v1.2$, $Na_v1.6$ (Maurice et al., 2001), β-actin, iNOS, cyclooxygenase-2 (COX-2), TNF-α, and IL-1β (Lee et al., 2004) and synthesized by the Genotech Corp (Daejeon, Korea), and the sequences of the primers were as follows (5′-3′): IL-1β forward, 5′-GCA GCT ACC TAT GTC TTG CCC GTG-3′, reverse, 5′-GTC GTT GCT TGT CTC TCC TTG TA-3′ (289 bp, 50°C for 30 cycles); TNF-α forward, 5′-CCC AGA CCC TCA CAC TCA GAT-3′; reverse, 5′-TTG TCC CTT GAA GAG AAC CTG-3′ (215 bp, 56°C for 28 cycles); COX-2 forward, 5′-CCA TGT CAA AAC CGT GGT GAA TG-3′; reverse, 5′-ATG GGA GTT GGG CAG TCA TCA G-3′ (374 bp, 55°C for 28 cycles); iNOS forward, 5′-CTC CAT GAC TCT CAG CAC AGA G-3′; reverse, 5′-GCA CCG AAG ATA TCC TCA TGA T-3′ (401 bp, 56°C for 25 cycles); $Na_v1.1$ forward, 5′-GAC CGG GTG ACA AAG CCA ATC-3′, reverse, 5′-CCCTTTACGCTGGTCCCTACAGTCT-3′ (353 bp, 58°C for 35 cycles); $Na_v1.2$ forward, 5′-CCT TCC ACA ACT TCT CCA CCT TCC TA-3′, reverse, 5′-ATA TGG CAG GTG TGG CAG TTA AAA CA-3′ (532 bp, 56°C for 23 cycles); $Na_v1.6$ forward, 5′-AGA GGT CAG GGA GTC CAA GTG CTA-3′, reverse, 5′-CGTCTGCCCAAGCGATAGGAG-3′ (256 bp, 60°C for 35 cycles); β-actin forward, 5′-AAC TTT GGC ATT GTG GAA GG-3′; reverse, 5′-GGA GAC AAC CTG GTC CTC AG-3′ (351 bp, 58°C for 23 cycles). After amplification, PCR products were subjected to a 2% agarose gel electrophoresis and visualized by ethidium bromide staining. The relative density of each band was analyzed by the ChemiImager™ 4400 (Alpha Innotech, San Leandro, CA). Experiments were repeated three times and the values obtained for the relative intensity were subjected to statistical analysis. The gels shown in figures are representative of results from three separate experiments.

EMSA

Primary microglia were lysed in ice-cold hypotonic lysis buffer (10 mM HEPES, pH 7.8, 10 mM KCl, 2 mM $MgCl_2$, 1 mM dithiothreitol (DTT), 0.1 mM ethylenediaminetetraacetic acid (EDTA), 0.1 mM phenylmethanesulfonylfluoride (PMSF), 1 μg/mL aprotinin, 10 μg/mL leupeptin). After 15 min, 0.5% NP-40 was added; nuclei were collected at 10,000*g* for 1 min, resuspended in hypertonic extraction buffer (50 mM HEPES, pH 7.8, 50 mM KCl, 300 mM NaCl, 0.1 mM PMSF), and centrifuged at 10,000*g* for 10 min. Supernatants were subjected to electrophoretic mobility shift assay (EMSA). After quantification of protein, the nuclear extracts were used in an EMSA assay described previously (Yune et al., 2004). In brief, oligonucleotide (0.3 pmole) for nuclear factor kappa-B (NF-κB) containing consensus binding sequence (Santa Cruz Biotechnology, Santa Cruz, CA) was radiolabeled with [γ-^{32}P]-dATP (GE Healthcare, Little Chalfont, UK) by T4 polynucleotide kinase (New England Biolabs, Beverly, MA) to produce double-stranded DNA probes. Ten micrograms of nuclear proteins were added to 20 μL of binding buffer (1 mM $MgCl_2$, 4% glycerol, 0.5 mM EDTA, 0.5 mM DTT, 50 mM NaCl, 1 μg of poly (dI-dC) and 10 mM Tris-HCl, pH7.5) containing ^{32}P-labeled double-stranded DNA (100,000 cpm) and incubated at room temperature for 20 min.

After incubation, bound and free probes were separated by electrophoresis on 6% polyacrylamide gel in non-denaturing condition and visualized by autoradiography. For competition experiments, radiolabeled DNA probes and nuclear proteins were incubated with a 100-fold molar excess of the unlabeled DNA oligonucleotide. Supershift assays were performed by preincubating nuclear extracts with polyclonal antibody against p65 subunits of NF-κB (Santa Cruz Biotechnology, Santa Cruz, CA) for 1 h on ice before adding labeled probes.

Western Blot

Total protein from primary microglia and injured spinal cord was prepared by homogenizing in ice-cold lysis buffer containing 1% Nonidet P-40, 20 mM Tris, pH 8.0, 137 mM NaCl, 0.5 mM EDTA, 10% glycerol, 10 mM $Na_2P_2O_7$, 10 mM NaF, 1 μg/mL aprotinin, 10 μg/mL leupeptin, 1 mM sodium vanadate, and 1 mM PMSF. Homogenates were incubated for 20 min at 4 C, and centrifuged at 25,000*g* for 30 min at 4 C. The protein level of the supernatant was determined using the BCA assay (Pierce, Rockford, IL). Protein samples (40 μg) were separated on SDS-PAGE and transferred to nitrocellulose membrane. The membranes were washed with TBS solution and blocked in 5% non fat skim milk or 5% bovine serum albumin in TBS-T (0.1% Tween 20) for 1 h at room temperature followed by incubation with antibodies against p38 mitogen activated protein kinase (p38MAPK; 1:1,000, Cell Signaling Technology, Danvers, MA), p-p38MAPK (1:1,000, Cell Signaling Technology), c-Jun N-terminal kinases (JNK, 1:1,000, Cell Signaling Technology), p-JNK (1:1,000, Cell Signaling Technology), iNOS (1:10,000, Transduction Laboratory, Lexington, KY), COX-2 (1:1,000, Cayman Chemicals Ann Arbor, MI), nuclear factor kappa-B (NF-κB; p65, 1:500, Santa Cruz Biotechnology), pro-nerve growth factor (proNGF, 1:200, Alomone Labs, Jerusalem, Israel), cleaved caspase-3 (1:200, Cell Signaling Technology), TNF-α, and IL-1β (1:400, Santa Cruz Biotechnology) at 4°C overnight. The primary antibodies were detected with horseradish peroxidase-conjugated secondary antibodies (Jackson ImmunoResearch, West Grove, PA). Immunoreactive bands were visualized by chemiluminescence using Supersignal (Thermo scientific, Rockford, IL). β-actin (1:2,000; Sigma), β-tubulin (1:10,000; Sigma) and Histon 1 (1:1,000, Cell Signaling Technology) were used as an internal control. Experiments were repeated three times and the densitometric values of the bands on Western blots obtained by MetaMorph software (Molecular devices). Background in films was subtracted from the optical density measurements.

Caspase-3 Activity

The caspase-3 enzyme activity was measured by using a caspase-3 assay kit (Millipore) as previously described (Kim et al., 2007). The specific activity of the samples was calculated relative to a standard curve using recombinant caspase-3 (Millipore). Experiments were carried out three times to ensure reproducibility.

TUNEL

Terminal deoxynucleotidyl transferase-mediated deoxyuridine triphosphate-biotin nick end labeling (TUNEL) staining was performed by using an Apoptag *in situ* kit (Millipore) according to the manufacturer's instructions as described (Yune et al., 2007). In brief, cells fixed in 4% paraformaldehyde were quenched with 3% H_2O_2. Thereafter, samples were incubated in a mixture of terminal transferase, digoxygenin-dUTP in TdT buffer at 37°C for 2 h. After the reaction was terminated with stopping buffer, samples were incubated in peroxidase-antidigoxygenin antibody at 37°C for 30 min. Diaminobenzidine substrate kit (Vector Labs, Burlingame, CA) was used for peroxidase staining. Control cells were incubated in the absence of TdT enzyme. TUNEL-positive cells in four fields selected randomly of each well of primary cortical neuron/microglia co-culture were counted and quantified using a 20× objective. Only those cells showing morphological features of nuclear condensation and/or compartmentalization were counted as TUNEL-positive.

Immunohistochemistry

For immunostaining, fixed primary microglia were processed for immunohistochemisty with antibodies against $Na_v1.1$, $Na_v1.2$, and $Na_v1.6$ (1:400, Alomone Labs). After three washes in PBS for 5 min, cells were incubated in 0.5% hydrogen peroxide in PBS for 30 min to inhibit endogenous peroxidase activity. Cells were blocked in 5% normal serum and 0.1% Triton X-100 in PBS for 1 h at RT and then incubated with primary antibodies overnight at 4°C, followed by HRP-conjugated secondary antibodies (Dako, Carpinteria, CA). The ABC method was used to detect labeled cells using a Vectastain kit (Vector Labs). DAB served as the substrate for peroxidase. Images were collected using an Olympus microscope connected via CoolSNAP. The tissue sections were also processed for immunohistochemistry with antibodies against p-p38MAPK (1:1,000, Cell Signaling Technology), cleaved caspase-3 (1:100, Cell Signaling Technology), OX-42 (microglia marker, 1:100, Millipore), and CC1 (oligodendrocyte marker, 1:100, Millipore). Resting and activated microglia were classified and counted based on previous reports (Hains and Waxman, 2006; Yune et al., 2009). Briefly, using immunostaining with OX-42 antibody (Millipore), resting microglia displayed small compact somata bearing long, thin, and ramified processes. Activated microglia exhibited marked cellular hypertrophy and retraction of processes such that the process length was less than the diameter of the soma compartment. Quantitative analysis was performed by blinded investigators. For axon staining, spinal cord sections were stained using an antibody specific for 200-kDa neurofilament protein (NF200, 1:1000; Sigma) as previously described (Yune et al., 2007). For double labeling, fluorescein isothiocyanate (FITC) or cyanine 3-conjugated secondary antibodies (Jackson ImmunoResearch) were used. Also, nuclei were labeled with DAPI according to the protocol of the manufacturer (Invitrogen). For quantification of cleaved caspase-3-positive oligodendrocytes (cleaved caspase-3/CC1 double positive), serial transverse sections (10-μm thickness) were collected every 200 μm from rostral and caudal 4,000 μm to the lesion site ($n = 4$, total 40 sections per animal). Cleaved caspase-3/CC1-positive oligodendrocytes in the white matter (WM) of spinal cord in each section were counted and averaged.

Statistics

Patch clamping data are expressed as mean ± SEM and other data are presented as mean ± SD values, unless otherwise specified. Data

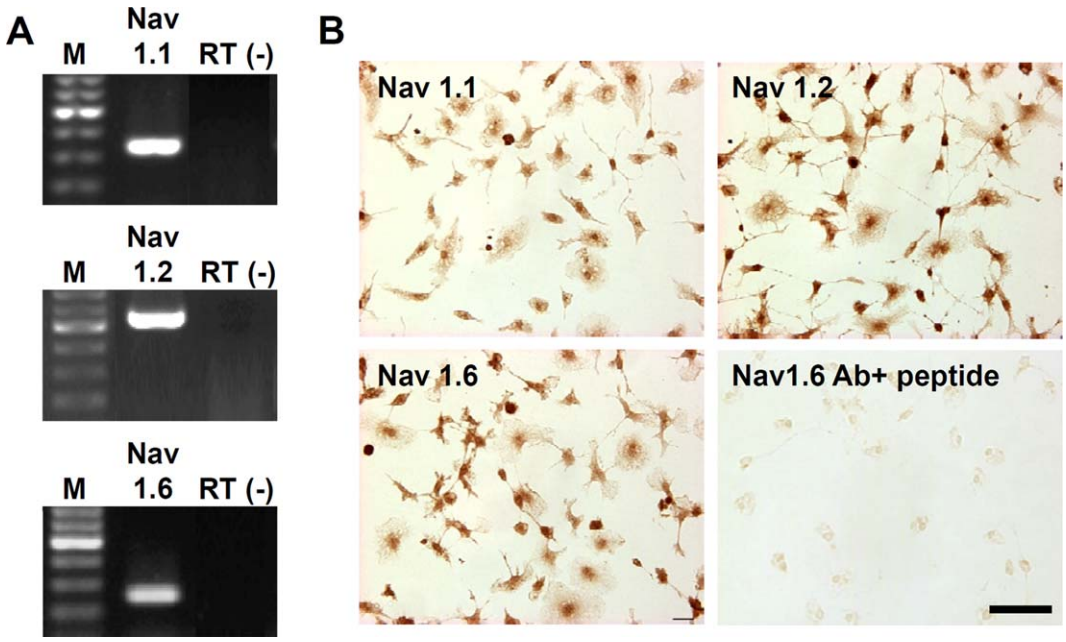

FIGURE 1: Primary microglia express isoforms of sodium channel $Na_v1.1$, $Na_v1.2$, and $Na_v1.6$. Primary microglia was cultured from the cerebral cortices of embryonic 17 d SD rat and total RNA and fixed cells were prepared described in Materials and Method section. RT-PCR (A) and immunohistochemistry (B) showed that isoforms of sodium channel, $Na_v1.1$, $Na_v1.2$, and $Na_v1.6$ were expressed in primary microglia. When primary antibody against $Na_v1.6$ was incubated with blocking peptide, $Na_v1.6$ immunoreactivity was disappeared, which showed the antibody specificity (B, bottom panel). Scale bar, 10 μm. [Color figure can be viewed in the online issue, which is available at wileyonlinelibrary.com.]

were evaluated for statistical significance using Student's paired *t*-test. In all analyses, a *P*-value of < 0.05 was considered statistically significant.

Results

Primary Microglia Express Isoforms of Sodium Channel, $Na_v1.1$, $Na_v1.2$, and $Na_v1.6$

Microglia are known to express a wide variety of ion channels, including K^+, Cl^-, H^+, and Ca^{2+} (Eder, 1998, 2005; Farber and Kettenmann, 2005; Illes et al., 1996). Microglia also express VGSC, which is categorized in TTX-sensitive and -insensitive (Korotzer and Cotman, 1992; Norenberg et al., 1994). In this study, we examined TTX-sensitive VGSCs: isoforms of $Na_v1.1$, $Na_v1.2$ and $Na_v1.6$, since they are known to be abundant in adult rodent CNS (Yu and Catterall, 2003). To identify the isoforms of sodium channels in primary microglia, we used RT-PCR (annealing temperature at 58°C) to detect α-subunit mRNAs of $Na_v1.1$, $Na_v1.2$, and $Na_v1.6$. The results showed that $Na_v1.1$, $Na_v1.2$ and $Na_v1.6$ were expressed in rat primary microglia (Fig. 1A), whereas other TTX-sensitive VGSCs such as $Na_v1.3$ and $Na_v1.7$ were not (data not shown). In addition, we found that the expression of sodium channels was not observed in astrocytes (data not shown). Immunocytochemistry with antibodies against $Na_v1.1$, $Na_v1.2$, and $Na_v1.6$ also showed that $Na_v1.1$, $Na_v1.2$, and $Na_v1.6$ were expressed in primary microglia (Fig. 1B). When primary antibody against $Na_v1.6$ was incubated with blocking peptide, $Na_v1.6$ immunoreactivity was disappeared, which showed the antibody specificity (Fig. 1B, right bottom panel). We got the same results when primary antibodies of $Na_v1.1$ and 1.2 were incubated with blocking peptide against each antibody (data not shown).

LPS Increases Inward Current of VGSC in Primary Microglia

Sodium channel is implicated in activation of microglia and macrophages in experimental autoimmune encephalomyelitis and multiple sclerosis lesions (Craner et al., 2005), and sodium channel activity is also known to modulate multiple functions such as phagocytosis, cytokine release, and migration in microglia (Black et al., 2009, 2012). However, whether the change in sodium influx would occur during microglia activation is largely unknown, although electrophysiological recordings of VGSC in normal rat and human microglia have already been reported (Korotzer and Cotman, 1992; Norenberg et al., 1994). Thus, we examined whether sodium current would increase when microglia were activated by LPS. When the membrane was depolarized, typical inward currents of VGSC are detected in rat primary microglia as reported (Korotzer and Cotman, 1992), which was completely blocked by perfused TTX (1 μM) treatment (Fig. 2A,B). LPS (1 μg/mL) treatment also resulted in further increases in sodium current (Fig. 2C,D). When expressed as a current density, LPS significantly increased current density

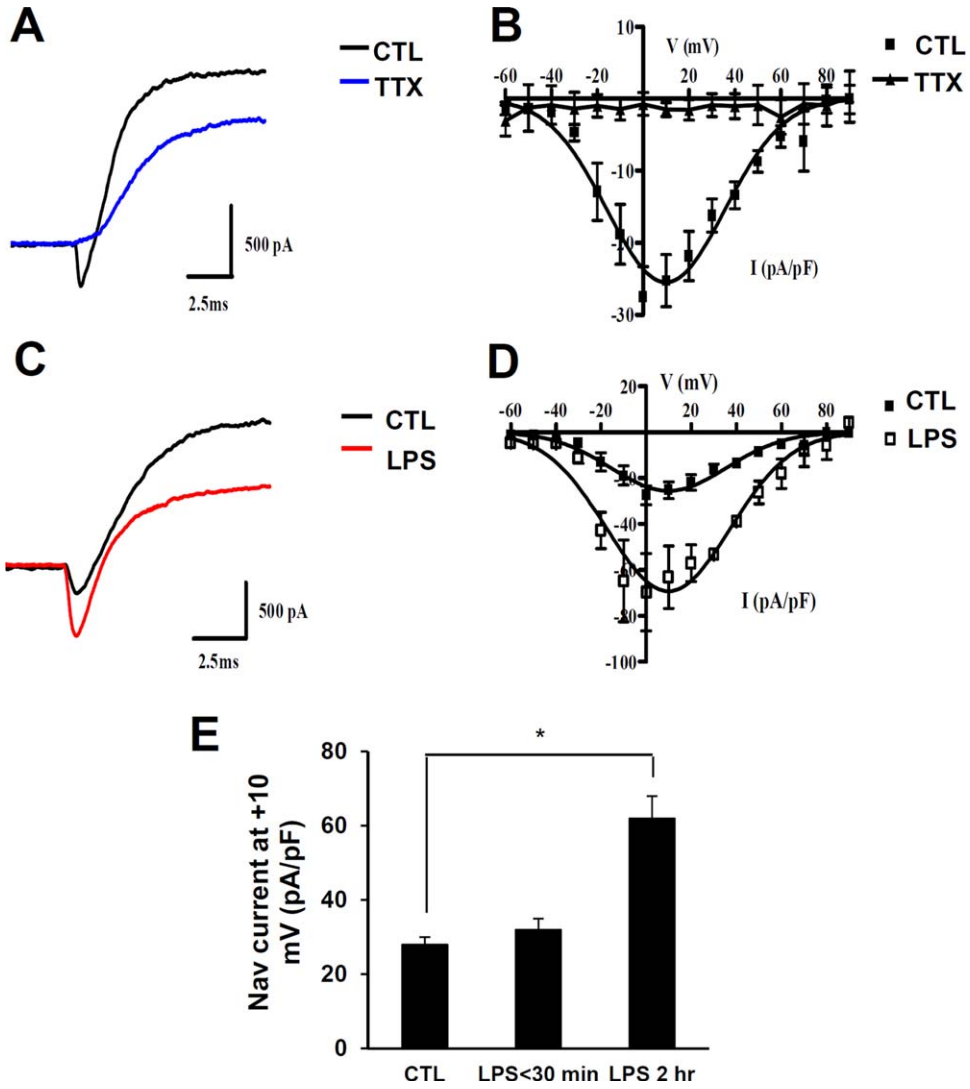

FIGURE 2: LPS increases inward currents of VGSC. Standard whole-cell recordings were made from rat primary microglia (A). The membrane potential was held at −80 mV, and peak inward current density is plotted in normal bath solution and in TTX (1 μM). Voltage steps were applied between −60 and +90 mV in 10 mV increments (B). Current traces (C) and I–V curves (D) show that sodium influx was further increased at 2 h after LPS treatment (1 μg/mL) (n = 8). Mean amplitude (±SEM) of inward currents of VGSC was measured at +10 mV and normalized to the cell capacitance. Current density (E) also show that LPS significantly increased current density from 27 ± 2.43 to 62.6 ± 9.28 pA/pF (n = 5). Data are presented as the mean ± SEM. *P < 0.05. [Color figure can be viewed in the online issue, which is available at wileyonlinelibrary.com.]

from 27 ± 2.43 to 62.6 ± 9.28 pA/pF (Fig. 2E). These results show that the sodium influx via VGSCs increases when microglia are activated by LPS. Interestingly, we also observed that LPS decreased outward K^+ currents under our recording conditions (Fig. 2C).

TTX Inhibits Expression of Inflammatory Mediators in LPS-Activated Microglia

Since the inward current of VGSC was increased when microglia was activated by LPS, we anticipated that blocking VGSC would also inhibit inflammatory responses in LPS-activated microglia. To examine whether TTX would inhibit expression of LPS-induced proinflammatory cytokines such as TNF-α, IL-1β or inflammatory mediators such as iNOS and COX-2, primary microglia cultures were treated with LPS (1 μg/mL) in the absence or presence of TTX (1 μM). As shown in Fig. 3A, the expression of TNF-α and IL-1β mRNA at 2 h and iNOS and COX-2 mRNA at 24 h after LPS treatment increased, which were inhibited by TTX. On Western blot analysis, the protein expression TNF-α and proIL-1β (31 kDa) at 6 h and iNOS and COX-2 at 24 h after LPS was also inhibited by TTX (Fig. 3B). However, we did not detect the mature form IL-1β (17.5 kDa) in the cell lysates (data not shown) as in previous report (Kim et al., 2004). In addition, the level of NO was increased by LPS treatment, which was significantly reduced by TTX (CTR,

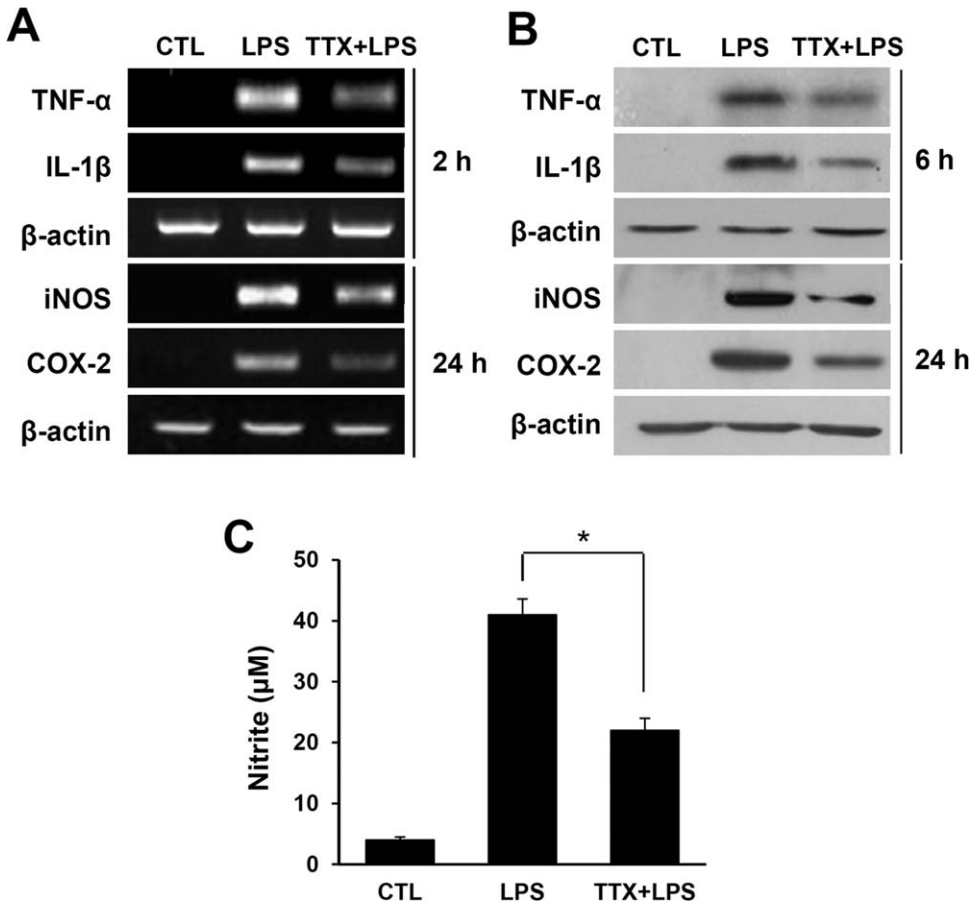

FIGURE 3: TTX inhibits LPS-induced expression of proinflammatory cytokines and inflammatory mediators. The levels of mRNA of TNF-α, IL-1β, COX-2, and iNOS (A) and protein of TNF-α, proIL-1β, COX-2, and iNOS (B) were increased in microglia by LPS treatment, which were significantly inhibited by TTX pretreatment for 30 min (1 μM). β-actin was used as an internal control. (C) NO production from culture media was determined by Griess reagent. Data indicated that TTX inhibited NO production at 24 h after LPS treatment. Values are mean ± SD of three separate experiments. *$P < 0.05$.

5.14 ± 0.56 *vs.* LPS, 43.61 ± 1.34 *vs.* TTX + LPS, 22.48 ± 1.39 μM, $P < 0.05$) (Fig. 3C). The basal level of NO was also detected in control group, although both iNOS mRNA and protein seem not to be expressed in the control group (Fig. 3A,B). This result seems to be attributable to the different analysis tool. Taken together, these data indicate that blocking of sodium influx inhibits inflammatory responses in LPS-activated microglia. However, TTX treatment alone didn't affect the level of NO in microglia (data not shown).

TTX Prevents Both NF-κB Translocation and p38MAPK Activation

NF-κB as a transcription factor is known to play a pivotal role in inflammatory responses such as expression of cytokines, iNOS, and COX-2, in activated microglia (Akira and Takeda, 2004). To examine NF-κB activation, microglia were treated with LPS in the absence or presence of TTX, and cytoplasmic and nuclear extracts were prepared as described in Materials and Method section. We first examined the translocation of NF-κB (p65) into nucleus by using fractionated cellular extract and whether TTX would modulate this event. Western blot showed that the nuclear translocation of p65 was increased by LPS treatment as compared with control while TTX inhibited its translocation (Fig. 4A). Next we confirmed this result by EMSA study. As shown in Fig. 4B, the radioactivity of NF-κB (p65/p50 and p50/p50) was increased by LPS treatment as compared with control, and TTX treatment reduced its radioactivity. The specificity of EMSA study of NF-κB was confirmed by observing the shift of p65 when p65 antibody was applied, which mean the binding of p65 to its DNA-responsive elements (Fig. 4B). By quantificative analysis of relative intensity of p65/p50, TTX significantly inhibited NF-κB activation when compared with LPS-treated sample (LPS, 6.2 ± 0.3 *vs.* TTX, 2.4 ± 0.5, $P < 0.05$) (Fig. 4C).

In addition, p38MAPK is also known to be involved in the production of cytokines, NO, and proNGF in activated microglia (Yune et al., 2007). Our previous report shows that p38MAPK-dependent proNGF production in microglia

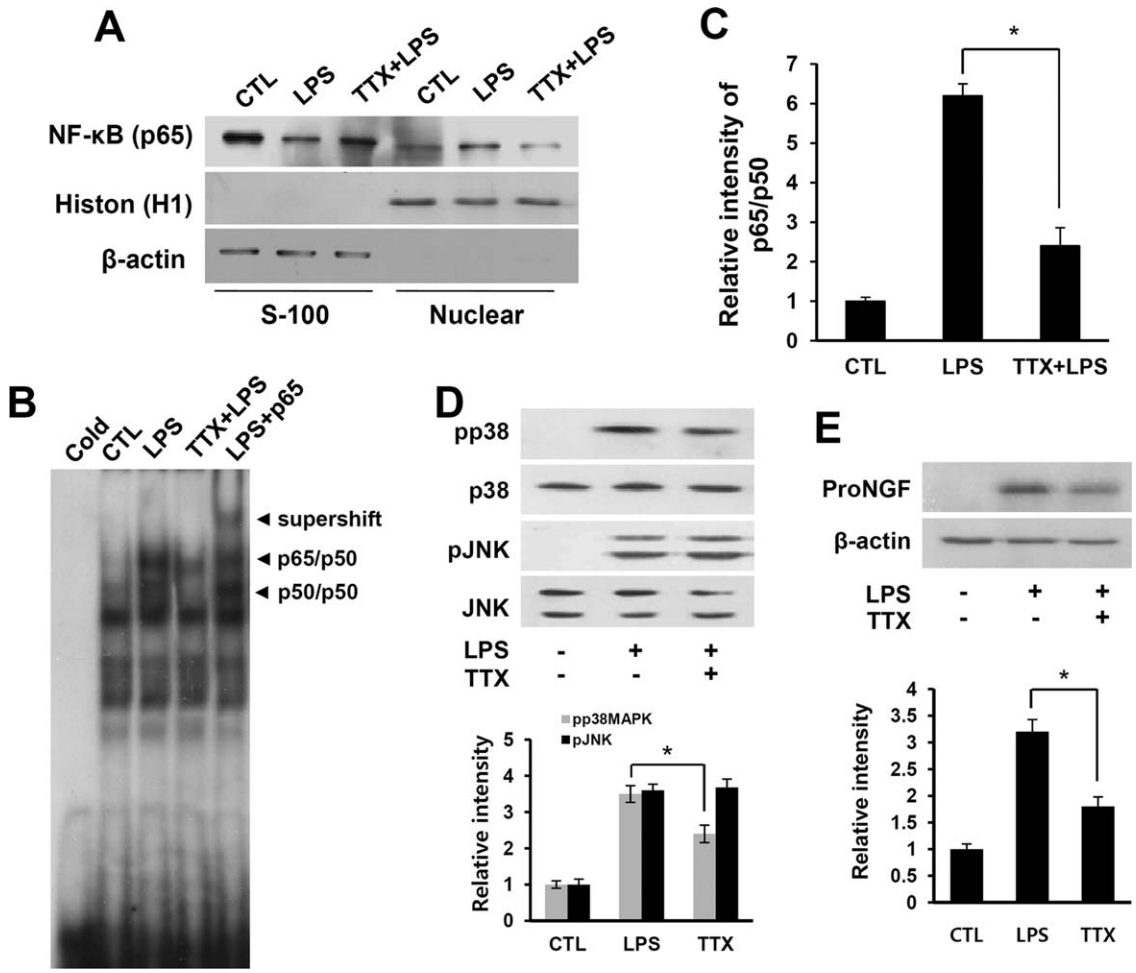

FIGURE 4: TTX inhibits LPS-induced NF-κB and p38MAPK activation in microglia. Nuclear and cytoplasmic extracts were prepared from microglia at 2 h after LPS treatment and NF-KB activation was assessed by Western blot and EMSA study. LPS treatment increased the level of NF-KB translocated into nucleus from cytoplasm, which was inhibited by TTX treatment (A). (B) EMSA analysis also showed that NF-κB binding in nuclear extracts was increased by LPS treatment, which was alleviated by TTX. (C) Quantification of p65/p50 complex of EMSA data showed that LPS-induced increase in NF-κB binding activity was inhibited by TTX. To assess the effect of TTX on MAPKs activation and proNGF expression, primary microglia were pretreated with TTX and then harvested at 2 h after LPS treatment. (D) Western blot showed that TTX significantly reduced the level of LPS-induced pp38MAPK in microglia, whereas the level of pJNK was not inhibited by TTX. (E) LPS-induced proNGF expression was also significantly inhibited by TTX. The gels shown are the representative of results from three separate experiments. β-actin and histone were used as internal controls. Data are presented as the mean ± SD of three separate experiments. *$P < 0.05$.

mediates oligodendrocyte cell death after SCI (23). Thus, we examined whether blocking of sodium channel would affect p38MAPK activation followed proNGF production when primary microglia was activated by LPS. As shown in Fig. 4D, LPS treatment increased the level pp38MAPK with the peak level at 2 h, which was significantly inhibited by TTX. However, JNK activation in LPS-activated microglia was not inhibited by TTX (p-p38MAPK: LPS, 3.4 ± 0.2 *vs.* TTX + LPS, 2.3 ± 0.25; pJNK: LPS, 3.6 ± 0.18 *vs.* TTX + LPS, 3.7 ± 0.27, $P < 0.05$) (Fig. 4D), although JNK is also known to be involved in cytokine production in microglia activated by LPS (Waetzig et al., 2005). In addition, the level of proNGF was increased by LPS treatment and TTX significantly reduced its level (LPS, 3.2 ± 0.23 *vs.* TTX + LPS, 1.7 ± 0.2, $P < 0.05$) (Fig. 4E).

TTX Inhibits Apoptotic Cell Death of Primary Cortical Neuron Co-cultured with LPS-Treated Microglia

To examine the effect of microglia activation on apoptotic cell death of neurons, primary cortical neurons were co-cultured for 48 h with microglia pretreated with LPS with or without TTX (1 μM) for 1 h. To exclude the direct effect of TTX and LPS on neurons, microglia seeded to porous well inserts, treated with LPS with or without TTX, and then washed before placing them above neurons. To examine the

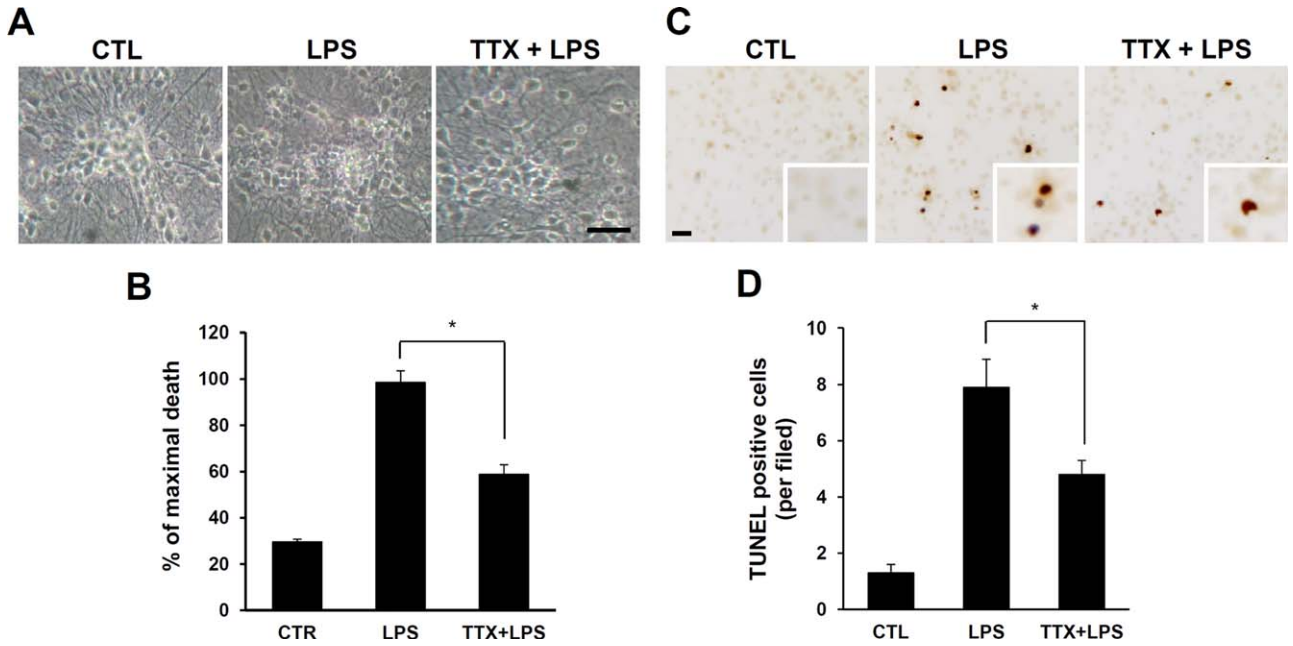

FIGURE 5: TTX protects primary cortical neurons from cytotoxicity and apoptotic cell death by LPS-induced microglial activation. Co-cultured primary cortical neurons with microglia were pretreated with TTX (1 μM) for 15 min before LPS (1 μg/mL) administration. After 48 h, cells and culture media were assayed for LDH release and TUNEL staining. Phase contrast photograph (A) and LDH assay (B) showed that TTX treatment significantly reduced LDH level, which means LPS-induced cytotoxicity was significantly inhibited by TTX. TUNEL staining (C) and quantification of TUNEL-positive cells (D) also showed that TUNEL-positive cell was not observed in control and the number of TUNEL-positive cells was increased by LPS treatment, which was significantly reduced by TTX. Values are mean ± SD of three separate experiments. Scale bar, 20 μm. *$P < 0.05$. [Color figure can be viewed in the online issue, which is available at wileyonlinelibrary.com.]

cytotoxicity, LDH assays were first performed after 48 h of neuron/microglia co-cultures. Results showed that incubation with LPS-stimulated microglia increased LDH release about five-fold as compared with control (Fig. 5A,B). Administration of TTX 15 min before LPS treatment resulted in significant reduction in LDH release (Fig. 5A,B). Neither LPS nor TTX treatment alone affected microglia or neuronal viability, as judged by LDH release (data not shown).

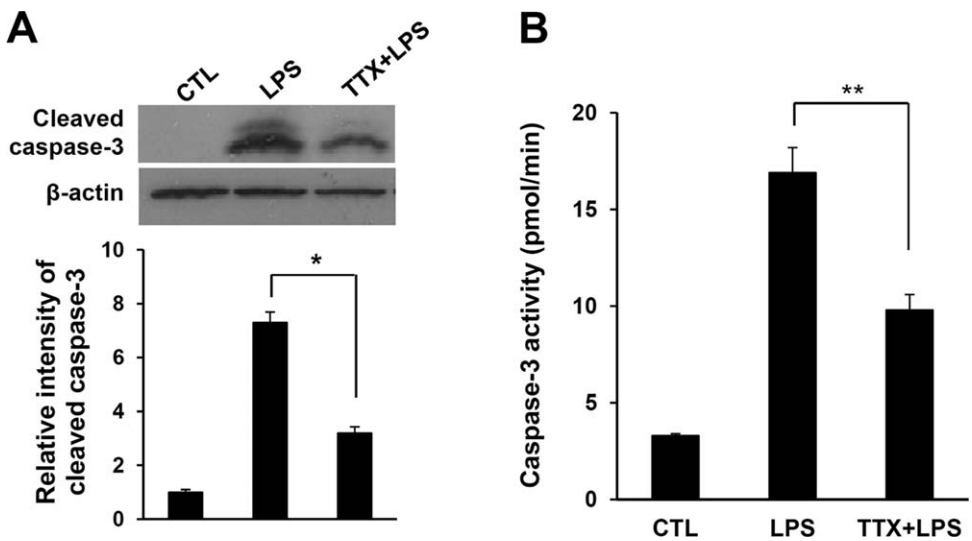

FIGURE 6: TTX inhibits LPS-induced caspase-3 activation in primary cortical neurons co-cultured with microglia. Co-cultured primary cortical neurons with microglia were pretreated with TTX (1 μM) for 15 min before LPS (1 μg/mL) treatment and after 48 h, cells were used for caspase-3 activation by Western blot and activity assay. (A) Western blot showed that the level of cleaved caspase-3 increased by LPS treatment was significantly alleviated by TTX treatment. (B) Caspase-3 activity measured by cleavage of Ac-DEVD in a fluorometric assay was also increased by LPS, which was significantly attenuated by TTX. Values are mean ± SD of four separate experiments. *$P < 0.01$, **$P < 0.05$.

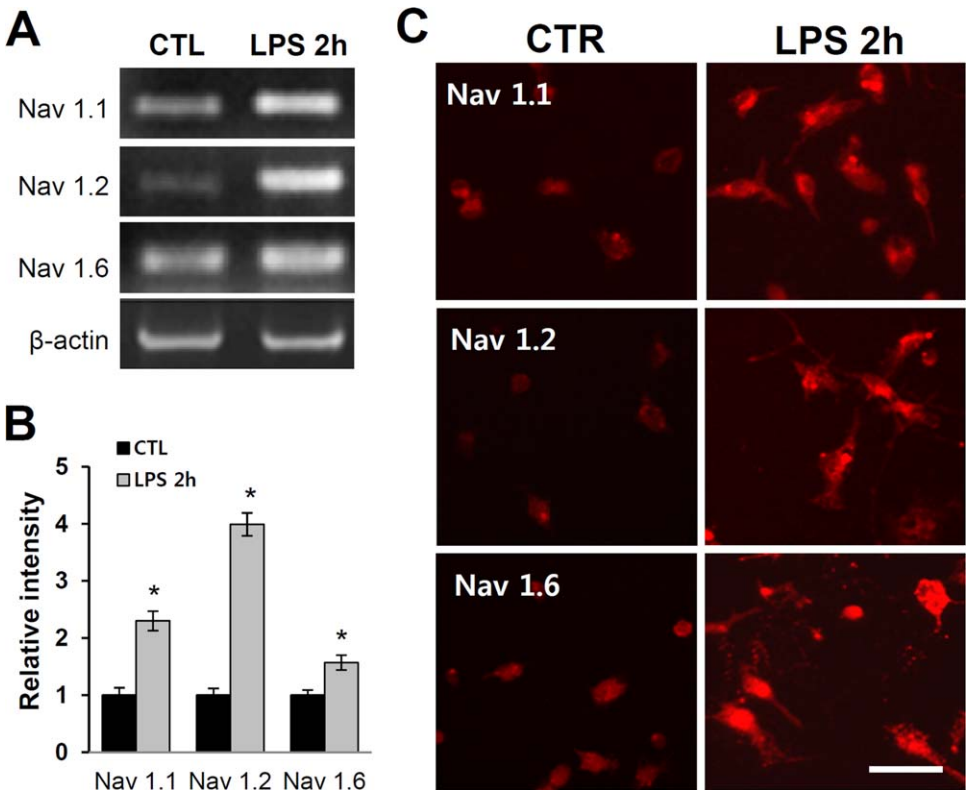

FIGURE 7: LPS treatment further increases the expression of sodium channels. RT-PCR for Nav 1.1, 1.2, and 1.6 (A), densitometric analysis (B), and immunofluorescence staining (C) show that LPS treatment up-regulated sodium channel expression at 2 h after LPS treatment. Values are mean ± SD of three separate experiments. Scale bar, 5 μm. *$P < 0.05$ *vs.* CTL. [Color figure can be viewed in the online issue, which is available at wileyonlinelibrary.com.]

Our previous report (Lee et al., 2004) show that microglia activated by LPS induce apoptotic cell death of neurons, as examined by TUNEL as well as caspase-3 activation. Thus we next assessed the apoptotic neuronal cell death after 48 h incubation with activated microglia by using TUNEL labeling. Compared with the increased number of TUNEL-positive neurons (7.8 ± 1.0 per field) induced by LPS-activated microglia, TTX significantly inhibited neuronal apoptotic cell death (4.3 ± 0.5 per field) (Fig. 5C,D). In addition, Western blot showed that the level of active caspase-3 increased by incubation with LPS-activated microglia, which was significantly reduced by TTX treatment (LPS, 7.3 ± 0.39 *vs.* TTX + LPS, 3.2 ± 0.23, $P < 0.05$) (Fig. 6A). Caspase-3 activity also increased by incubation with LPS-activated microglia, whereas pretreatment with TTX resulted in a 45% reduction of caspase-3 activity (CTL, 3.3 ± 0.1 *vs.* LPS, 16.9 ± 1.3 *vs.* TTX + LPS, 9.8 ± 0.8, $P < 0.01$) (Fig. 6B).

LPS Treatment Further Increases the Expression of Sodium Channels in Microglia

Next we examined the change in sodium channel expression in microglia when the cells were activated by LPS. As shown in Fig. 7A,B, the expression of sodium channels (Nav1.1, Nav1.2, and Nav1.6) mRNA was significantly further increased in microglia at 2 h activated by LPS (Nav1.1, 2.3 ± 0.17 fold; Nav1.2, 4.0 ± 0.2 fold; Nav 1.6 ± 0.13 fold *vs.* control, $P < 0.05$). Immunostaining with antibodies for Nav1.1, Nav1.2, and Nav1.6 also showed that the immunoreactivity of each sodium channel protein was increased at 2 h after LPS treatment as compared with control (Fig. 7C).

TTX Inhibits Microglia Activation and Oligodendrocyte Cell Death After Spinal Cord Injury

Our previous report also shows that p38MAPK-dependent proNGF production in activated microglia mediates oligodendrocyte cell death via $p75^{NTR}$ at 5 d after SCI (Yune et al., 2007). We also showed that TTX inhibited p38MAKP activation and proNGF production in activated microglia by LPS *in vitro* (Fig. 4D,E). Thus, we anticipated that TTX would inhibit microglia activation and oligodendrocyte cell death following SCI. TTX (0.15 nmole) was administered into the lesion epicenter after injury. Immunohistochemistry with OX-42 antibody showed that the number of morphologically activated microglia at 5 d after SCI was significantly reduced in TTX-treated spinal section as compared with vehicle control (Fig. 8A,B; Vehicle, 66.5 ± 5.2% *vs.* TTX, 29.6 ± 2.6%, $P < 0.05$). Immunohistochemistry and Western blot also

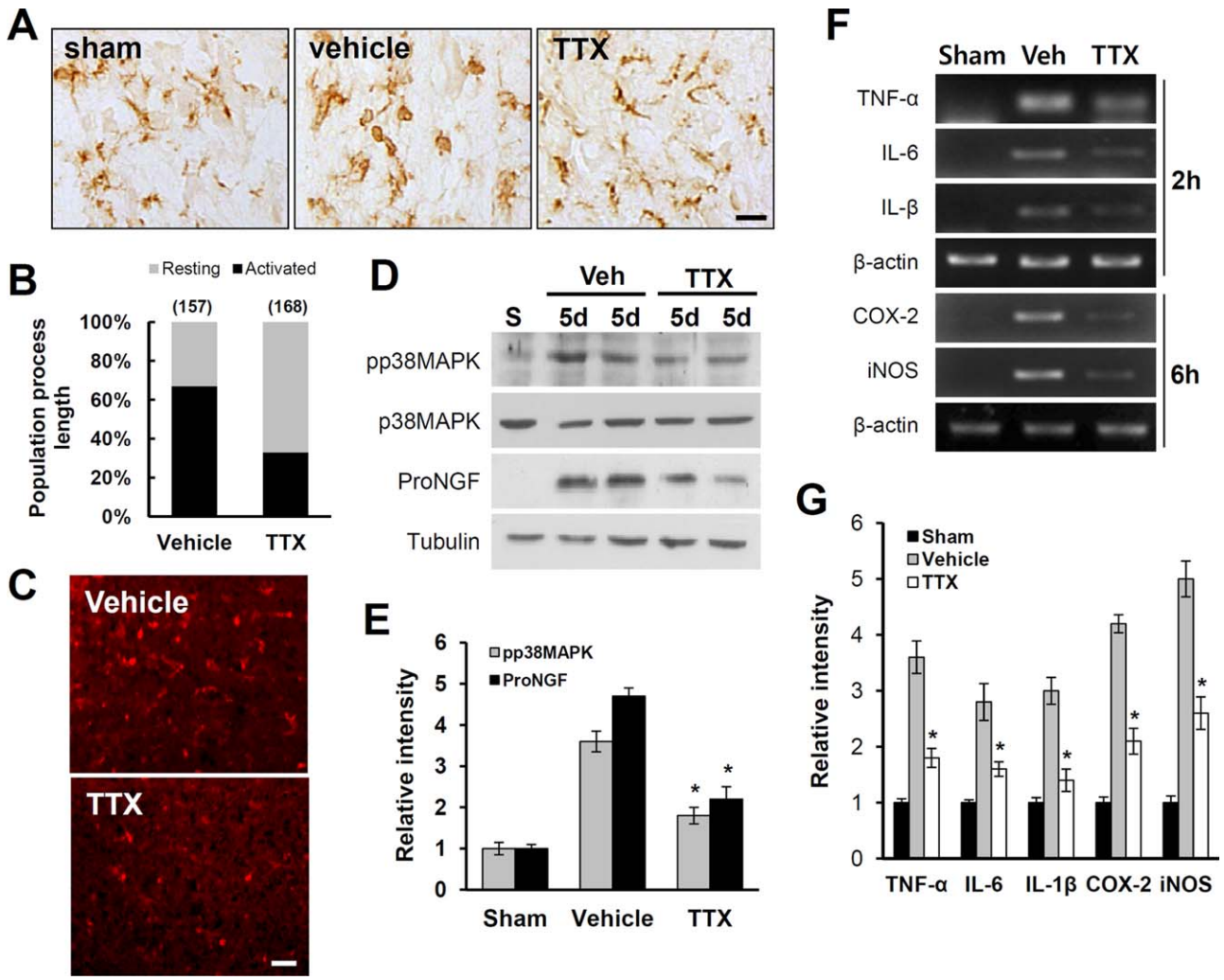

FIGURE 8: TTX inhibits microglial activation after SCI. (A) Immunohistochemistry with anti-OX-42 antibody and (B) quantification of activated and resting microglia in the 2000 μm rostral gray matter from lesion site at 5 d after SCI showed that intraspinal injection of TTX (0.15 nmole) after SCI significantly inhibited microglial activation. Scale bar, 20 μm. Immunohistochemistry with anti-pp38MAPK antibody (C), Western blot (D), and densitometric analysis (E) also show that p38MAPK activation and proNGF expression increased at 5 d after SCI also significantly inhibited by TTX. Scale bar, 20 μm. (F) The levels of mRNA of TNF-α, IL-6, IL-1β (at 2 h), COX-2, and iNOS (at 6 h) are markedly increased after SCI and significantly inhibited by TTX treatment. β-actin was used as an internal control. Values are mean ± SD (n = 4). *P < 0.05. [Color figure can be viewed in the online issue, which is available at wileyonlinelibrary.com.]

showed that the level of pp38MAPK and proNGF increased after SCI was significantly reduced in TTX-treated group at 5 d after injury when compared with vehicle control (p-p38MAPK: vehicle, 3.6 ± 0.33 *vs.*TTX, 1.9 ± 0.21, proNGF: vehicle, 4.9 ± 0.19 *vs.* TTX, 2.2 ± 0.25, $P <$ 0.05) (Fig. 8C–E). In addition, RT-PCR and quantitative analysis reveal that TTX treatment significantly inhibited the expression of proinflammatory cytokines and mediators such as TNF-α, IL-6, IL-1β, COX-2, and iNOS when compared with those in the vehicle-treated group (TNF-α: vehicle, 3.6 ± 0.29 *vs.* TTX, 1.8 ± 0.17; IL-6: vehicle, 2.8 ± 0.33 *vs.* TTX, 1.6 ± 0.13; IL-1β: vehicle, 3.0 ± 0.24 *vs.* TTX, 1.4 ± 0.2; COX-2: vehicle, 4.2 ± 0.16 *vs.* TTX, 2.1 ± 0.23; iNOS: vehicle, 5.0 ± 0.32 *vs.* TTX, 2.6 ± 0.29, $P <$ 0.05) (Fig. 8F,G). This *in vivo* study confirmed the *in vitro* data showing that VGSCs are involved in microglia activation.

Next, we examined the effect of TTX on oligodendrocyte cell death after SCI. As shown in Fig. 9, intraspinal microinjection of TTX (0.15 nmole) after SCI resulted in a significant decrease in the number of caspase-3^+/$CC1^+$-positive oligodendrocytes in the white matter (WM) of spinal cord at 5 d after SCI as compared with the vehicle control (Veh, 37 ± 1.8 *vs.* TTX, 24 ± 2.3, $P <$ 0.05). Western blot analysis also shows that TTX treatment significantly inhibited the level of cleaved (activated) forms of caspase-3 at 5 d after injury (vehicle, 5.4 ± 0.2 *vs.* TTX, 2.35 ± 0.31, $P <$ 0.05) (Fig. 9C,D). These results suggest that TTX may exert its neuroprotective effect on oligodendrocytes likely by blocking

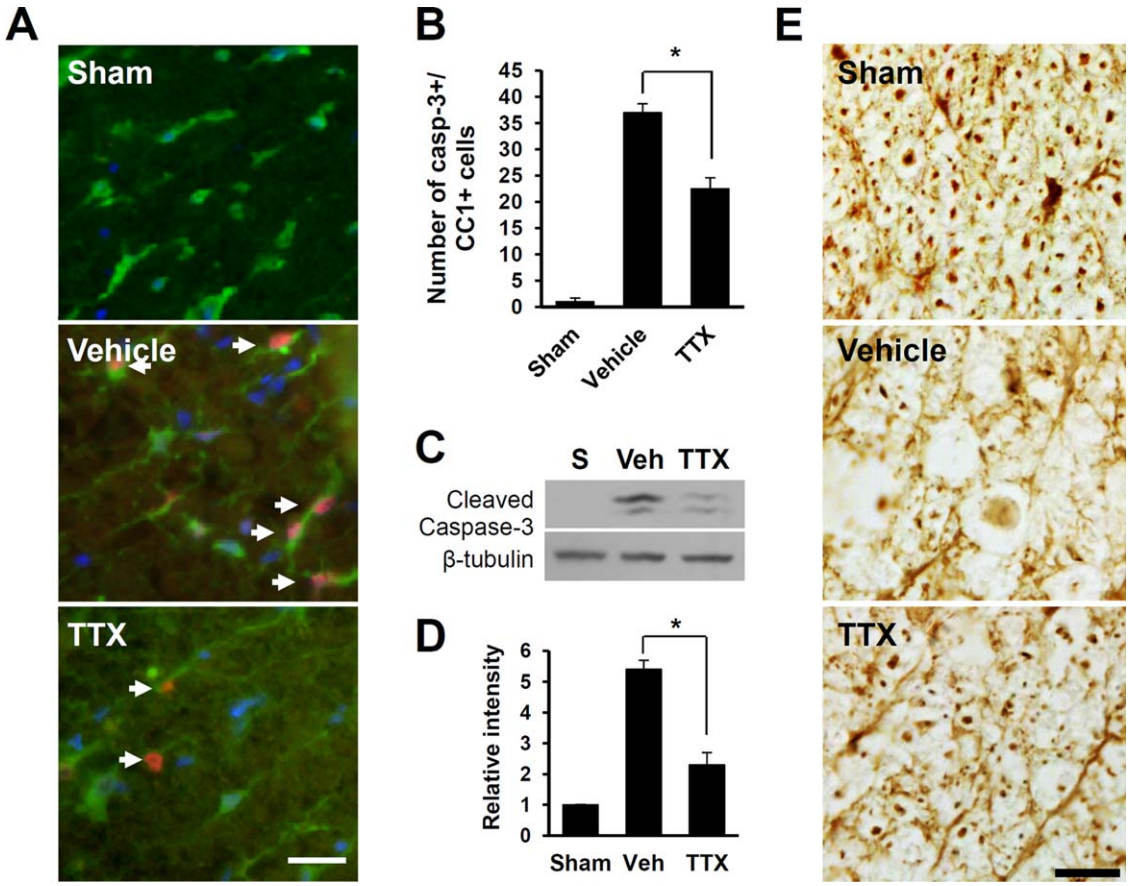

FIGURE 9: TTX inhibits apoptotic cell death of oligodendrocyte after SCI. Rats receiving the moderate injury were injected intraspinally with TTX (0.15 nmole). At 5 d after injury, spinal cord sections (transverse sections) were stained with triple labeling with cleaved caspase-3 in red, CC1 in green, and DAPI in blue. (A) Double immunofluorescence staining and (B) Quantification analyses show that TTX treatment significantly reduced the number of caspase-3/CC1-positive oligodendrocytes in the WM as compared with vehicle control. Serial transverse sections (10-μm thickness) collected every 200 μm from rostral and caudal 4,000 μm to the lesion site (n = 4, total 40 sections per animal) were used for quantification. Representative images were from the sections selected 2-mm rostral to the lesion epicenter. Arrows indicate caspase-3/CC1-positive cells. Values are mean ± SD (n = 4). Scale bar, 20 μm. *P < 0.05. (C) Western blots of caspase-3 at 5 d after injury. (D) Quantitative analysis of Western blots show that TTX treatment significantly inhibited caspase-3 activation after injury. Values are mean ± SD (n = 4). *P < 0.05. (E) Representative photographs of NF200-positive axons in sham, vehicle and TTX-treated spinal sections 1 mm rostral to the lesion epicenter at 5 d. Scale bar, 20 μm. [Color figure can be viewed in the online issue, which is available at wileyonlinelibrary.com.]

VGSCs in microglia after injury. Finally, we found that TTX treatment also attenuated axon loss at 5 d after SCI (Fig. 9E).

Discussion

In this study, we found that an increase in sodium influx via voltage-gated sodium channel (VGSC) in microglia was preceded microglia activation followed inflammatory responses. $Na_v1.1$, $Na_v1.2$, and $Na_v1.6$ were expressed in primary microglia and the inward current of VGSC was increased in response to LPS, which was completely blocked by sodium channel blocker, TTX. Our data also showed that TTX inhibited TNF-α, IL-1β, COX-2, and iNOS expression and NO production in microglia activated by LPS, which resulted in the inhibition of LPS-induced caspase-3 activation and neuronal cell death in neuron/microglia co-cultures. In addition, we found that the inhibition of inflammatory mediator expression by TTX was mediated by inhibiting NF-κB translocation from cytoplasm to nucleus and p38MAPK activation after LPS treatment in primary microglia. Furthermore, LPS treatment further increase of sodium channels expression in microglia. Finally, our data showed that TTX treatment inhibited microglia activation, p38MAPK activation followed proNGF production, and the expression of inflammatory mediators such as TNF-α, IL-1β, IL-6, COX-2, and iNOS after SCI. As in *in vitro* study, caspase-3 activation and apoptotic cell death of oligodendrocyte after SCI were also significantly alleviated by TTX treatment.

VGSC are expressed in various cells such as excitable neurons and muscle cells, which function initiation and propagation of action potentials (Hodgkin et al., 1952), and also in non-excitable astrocytes, immune cells, and microglia (Eder, 1998; Fraser et al., 2004; Korotzer and Cotman, 1992;

Lai et al., 2000; Norenberg et al., 1994; Sontheimer et al., 1994). However, the function and role of VGSC in non-excitable cells on cellular processes have not been fully elucidated. At least, 10 VGSCs α-subunit isoforms are identified and three of these ($Na_v1.1$, $Na_v1.2$, and $Na_v1.6$) are known to be expressed at high levels in the adult central nervous system (Catterall et al., 2005; Yu and Catterall, 2003). $Na_v1.1$, $Na_v1.2$ and $Na_v1.6$ are TTX-sensitive, and therefore we focused on these channels in this study to elucidate the function of VGSCs in microglia activation followed inflammatory responses and apoptotic cell death in *in vitro* and *in vivo*. Our RT-PCR and immunohistochemistry showed that $Na_v1.1$, $Na_v1.2$, and $Na_v1.6$ were expressed in primary microglia (see Fig. 1) while other TTX-sensitive VGSCs such as $Na_v1.3$ and $Na_v1.7$ was not expressed (data not shown). However, Black et al. (2009) reported that $Na_v1.1$, $Na_v1.5$, and $Na_v1.6$ are detectable by immunolabeling, whereas $Na_v1.2$, $Na_v1.3$, $Na_v1.7$, $Na_v1.8$, and $Na_v1.9$ are not in primary microglia. Although we did not examine other isoforms of sodium channel, there is a discrepancy in the expression of $Na_v1.2$ between our data and the report by Black et al (2009). Perhaps, we postulate that such discrepancy may be resulted from the culture condition, microglial status or the source of animals of primary microglia.

Existence of VGSC in microglia has been demonstrated by electrophysiological techniques in rodent and human microglia (Korotzer and Cotman, 1992; Norenberg et al., 1994), and sodium channel activity is known to modulate multiple functions such as phagocytosis, cytokine release, and migration in microglia (Black et al., 2009; Black and Waxman, 2012). However, the direct physiological and molecular evidence demonstrating the change of VGSC current and expression in microglia has not been shown yet. Our data showed that sodium current via VGSCs was observed when the membrane of microglia was depolarized as reported (Korotzer and Cotman, 1992; Norenberg et al., 1994), and sodium influx current was further increased when microglia were activated by LPS treatment, which was completely blocked by TTX treatment (see Fig. 2). Furthermore, we elucidated the role of VGSC on microglia activation followed inflammation in *in vivo* study. This is the first study to evaluate the role of VGSC on microglia activation and oligodendrocytes cell death after SCI. It is interesting to observe the inhibitory effect of LPS on outward K^+ current as shown in Fig. 2C. However, further investigation is necessary to understand the role and types of K^+ currents observed in activated microglia by LPS.

It has been known that after SCI, the level of adenosine neucletide including ATP is changed. Especially, extracellular ATP seems to be a key molecule for triggering microglial response to pathological events, initiating and maintaining reactive microglia via ionotropic P2X receptor subfamilies (Lu et al., 2013; Shigemoto-Mogami et al., 2001; Trang et al., 2009; Wang et al., 2004). Recent repot showed that ATP treatment increases the migration of microglia and sodium channel blockers such as phenytoin or TTX inhibits ATP-induced migration of microglia in primary microglia culture (Black et al., 2009). In this study, we did not observe any change of sodium current by ATP in our culture condition, although ATP treatment increased the expression of inflammatory cytokines as in a previous report (Li et al., 2013; Shigemoto-Mogami et al., 2001) (data not shown). However, we cannot rule out the potential effect of ATP on sodium current in microglia.

In acute or chronic neurodegenerative diseases, various stimuli such as α-synuclein (Zhang et al., 2005), β-amyloid (Qin et al., 2002), matrix metalloproteinase-3 (Kim et al., 2005), and neuromelanin (Wilms et al., 2003) from damaged neurons, thrombin (Ryu et al., 2000) and cytokines from infiltrating cells, and cellular membrane components of bacteria (Block and Hong, 2005; Koistinaho and Koistinaho, 2002) activate microglia by binding receptors and lead to dramatic phenotypic and functional changes. In this study, we used LPS as an activator of microglia. It is well known that LPS binding to Toll-like receptor 4 (TLR-4) on microglia activates multiple signaling pathways (Akira and Takeda, 2004; Palsson-McDermott and O'Neill, 2004). MAPK is one of key signaling molecules in LPS-induced cytokines and inflammatory mediator expression (Koistinaho and Koistinaho, 2002; Waetzig et al., 2005). As possible mechanisms involved in the anti-inflammatory effect by blocking sodium channels, we found that TTX inhibited LPS-induced p38MAPK activation in primary microglia (see Fig. 4D). However, JNK activation was not affected by TTX. In addition, NF-κB activation is another hallmark of microglia activation after LPS treatment. Upon serine phosphorylation of IκB protein by IKK, it is targeted for proteasome-mediated degradation, thus allowing NF-κB protein complex to translocate into the nucleus from cytoplasm where it can activate the gene expression of inflammatory mediators. Our study clearly demonstrated that LPS-induced NF-κB translocation was inhibited by TTX (see Fig. 4A–C). These findings suggest that an increase in sodium influx in microglia by LPS may instigate NF-κB and p38MAPK activation mediating expression of proinflammatory cytokines and inflammatory mediators.

Regulating neuronal sodium influx has been considered as a therapeutic strategy for preventing neurotoxicity. For example, sodium channel blockers, RS100642, 619C89, and riluzole, have shown neuroprotective effect in ischemic and traumatic brain injury as well as Parkinson's disease animal models by alleviating the excitotoxic effects (Barneoud et al., 1996; Sun and Faden, 1995; Williams and Tortella, 2002).

Sodium channels are also known to play a key role in axonal degeneration. For example, sodium channel blockers such as phenytoin (Hains et al., 2004; Lo et al., 2002), TTX (Rosenberg et al., 1999; Teng and Wrathall, 1997), and flecainide (Bechtold et al., 2004) are known to have protective effect on axons in SCI or multiple sclerosis animal models. We also found that TTX attenuated the loss of axons after SCI as in previous reports (see Fig. 9E). Based on our findings that blocking sodium channels in microglia inhibits inflammatory responses, we examined the neuroprotective effect of TTX by blocking microglia activation in *in vitro* and *in vivo*. Our data showed that TTX significantly inhibited LPS-induced cytotoxicity and apoptotic cell death in primary neuron/microglia co-culture (see Figs. 5 and 6). Furthermore, TTX treatment inhibited microglial activation at 5 d after SCI and p38MAPK activation followed proNGF production, which resulted in inhibition of apoptotic cell death of oligodendrocytes (see Fig. 9). These results indicate that TTX treatment inhibits oligodendrocytes apoptosis after SCI in part by inhibiting microglial activation via blocking of sodium channel in microglia. However, we cannot rule out the possibility that blocking of sodium channels expressed in neurons by TTX may contribute to the inhibition of microglial activation followed oligodendrocytes cell death after injury. Furthermore, how TLR-4-mediated signaling pathway is linked to sodium influx via VSGC by LPS and/or whether TLR-4 interacts with VSGC will be required for further study.

In summary, our *in vivo* and *in vitro* results indicate that neuronal cell death can be mitigated by sodium channel blocker via inhibiting microglial inflammatory responses. The inhibitory effect of TTX on microglial proinflammatory cytokines and inflammatory mediator production resulted from the decreased NF-κB translocation and p38MAPK activation. Therefore, our results suggest that the increase in VGSC influx appears to be prerequisite to microglial activation after injury.

Acknowledgment

Grant sponsor: Pioneer Research Center Program, National Research Foundation of Korea funded by the Ministry of Science, ICT & Future Planning; Grantnumber: 2010-0019349; Grant sponsor: SRC, National Research Foundation of Korea funded by the Ministry of Science, ICT & Future Planning; Grant number: 2008-0061888; Grant sponsor: Grant of the Korea Health technology R&D Project, Ministry of Health & Welfare, Republic of Korea; Grant number: A101198.

References

Akira S, Takeda K. 2004. Toll-like receptor signalling. Nat Rev Immunol 4: 499–511.

Barneoud P, Mazadier M, Miquet JM, Parmentier S, Dubedat P, Doble A, Boireau A. 1996. Neuroprotective effects of riluzole on a model of Parkinson's disease in the rat. Neuroscience 74:971–983.

Beattie MS. 2004. Inflammation and apoptosis: Linked therapeutic targets in spinal cord injury. Trends Mol Med 10:580–583.

Beattie MS, Hermann GE, Rogers RC, Bresnahan JC. 2002. Cell death in models of spinal cord injury. Prog Brain Res 137:37–47.

Bechtold DA, Kapoor R, Smith KJ. 2004. Axonal protection using flecainide in experimental autoimmune encephalomyelitis. Ann Neurol 55:607–616.

Black JA, Liu S, Waxman SG. 2009. Sodium channel activity modulates multiple functions in microglia. Glia 57:1072–1081.

Black JA, Waxman SG. 2012. Sodium channels and microglial function. Exp Neurol 234:302–315.

Block ML, Hong JS. 2005. Microglia and inflammation-mediated neurodegeneration: Multiple triggers with a common mechanism. Prog Neurobiol 76:77–98.

Catterall WA, Goldin AL, Waxman SG. 2005. International Union of Pharmacology. XLVII. Nomenclature and structure-function relationships of voltage-gated sodium channels. Pharmacol Rev 57:397–409.

Chan CC. 2008. Inflammation: Beneficial or detrimental after spinal cord injury? Recent Pat CNS Drug Discov 3:189–199.

Colton CA. 2009. Heterogeneity of microglial activation in the innate immune response in the brain. J Neuroimmune Pharmacol 4:399–418.

Craner MJ, Damarjian TG, Liu S, Hains BC, Lo AC, Black JA, Newcombe J, Cuzner ML, Waxman SG. 2005. Sodium channels contribute to microglia/macrophage activation and function in EAE and MS. Glia 49:220–229.

David S, Kroner A. 2011. Repertoire of microglial and macrophage responses after spinal cord injury. Nat Rev Neurosci 12:388–399.

Donnelly DJ, Popovich PG. 2008. Inflammation and its role in neuroprotection, axonal regeneration and functional recovery after spinal cord injury. Exp Neurol 209:378–388.

Eder C. 1998. Ion channels in microglia (brain macrophages). Am J Physiol 275:C327–C342.

Eder C. 2005. Regulation of microglial behavior by ion channel activity. J Neurosci Res 81:314–321.

Farber K, Kettenmann H. 2005. Physiology of microglial cells. Brain Res Brain Res Rev 48:133–143.

Fraser SP, Diss JK, Lloyd LJ, Pani F, Chioni AM, George AJ, Djamgoz MB. 2004. T-lymphocyte invasiveness: Control by voltage-gated Na+ channel activity. FEBS Lett 569:191–194.

Hains BC, Saab CY, Lo AC, Waxman SG. 2004. Sodium channel blockade with phenytoin protects spinal cord axons, enhances axonal conduction, and improves functional motor recovery after contusion SCI. Exp Neurol 188:365–377.

Hains BC, Waxman SG. 2006. Activated microglia contribute to the maintenance of chronic pain after spinal cord injury. J Neurosci 26:4308–4317.

Hanisch UK, Kettenmann H. 2007. Microglia: Active sensor and versatile effector cells in the normal and pathologic brain. Nat Neurosci 10:1387–1394.

Hodgkin AL, Huxley AF, Katz B. 1952. Measurement of current-voltage relations in the membrane of the giant axon of Loligo. J Physiol 116:424–448.

Illes P, Norenberg W, Gebicke-Haerter PJ. 1996. Molecular mechanisms of microglial activation. B. Voltage- and purinoceptor-operated channels in microglia. Neurochem Int 29:13–24.

Kim SH, Smith CJ, Van Eldik LJ. 2004. Importance of MAPK pathways for microglial pro-inflammatory cytokine IL-1 beta production. Neurobiol Aging 25:431–439.

Kim SJ, Yune TY, Han CT, Kim YC, Oh YJ, Markelonis GJ, Oh TH. 2007. Mitochondrial isocitrate dehydrogenase protects human neuroblastoma SH-SY5Y cells against oxidative stress. J Neurosci Res 85:139–152.

Kim YS, Kim SS, Cho JJ, Choi DH, Hwang O, Shin DH, Chun HS, Beal MF, Joh TH. 2005. Matrix metalloproteinase-3: A novel signaling proteinase from apoptotic neuronal cells that activates microglia. J Neurosci 25:3701–3711.

Koistinaho M, Koistinaho J. 2002. Role of p38 and p44/42 mitogen-activated protein kinases in microglia. Glia 40:175–183.

Korotzer AR, Cotman CW. 1992. Voltage-gated currents expressed by rat microglia in culture. Glia 6:81–88.

Kreutzberg GW. 1996. Microglia: A sensor for pathological events in the CNS. Trends Neurosci 19:312–318.

Lai ZF, Chen YZ, Nishimura Y, Nishi K. 2000. An amiloride-sensitive and voltage-dependent Na+ channel in an HLA-DR-restricted human T cell clone. J Immunol 165:83–90.

Lee SM, Yune TY, Kim SJ, Kim YC, Oh YJ, Markelonis GJ, Oh TH. 2004. Minocycline inhibits apoptotic cell death via attenuation of TNF-alpha expression following iNOS/NO induction by lipopolysaccharide in neuron/glia co-cultures. J Neurochem 91:568–578.

Li J, Ren W, Huang XJ, Zou DJ, Hu X. 2013. Bullatine A, a diterpenoid alkaloid of the genus Aconitum, could attenuate ATP-induced BV-2 microglia death/apoptosis via P2X receptor pathways. Brain Res Bull 97C:81–85.

Lo AC, Black JA, Waxman SG. 2002. Neuroprotection of axons with phenytoin in experimental allergic encephalomyelitis. Neuroreport 13:1909–1912.

Lu WH, Wang CY, Chen PS, Wang JW, Chuang DM, Yang CS, Tzeng SF. 2013. Valproic acid attenuates microgliosis in injured spinal cord and purinergic P2X4 receptor expression in activated microglia. J Neurosci Res 91:694–705.

Maurice N, Tkatch T, Meisler M, Sprunger LK, Surmeier DJ. 2001. D1/D5 dopamine receptor activation differentially modulates rapidly inactivating and persistent sodium currents in prefrontal cortex pyramidal neurons. J Neurosci 21:2268–2277.

Norenberg W, Illes P, Gebicke-Haerter PJ. 1994. Sodium channel in isolated human brain macrophages (microglia). Glia 10:165–172.

Palsson-McDermott EM, O'Neill LA. 2004. Signal transduction by the lipopolysaccharide receptor, Toll-like receptor-4. Immunology 113:153–162.

Qin L, Liu Y, Cooper C, Liu B, Wilson B, Hong JS. 2002. Microglia enhance beta-amyloid peptide-induced toxicity in cortical and mesencephalic neurons by producing reactive oxygen species. J Neurochem 83:973–983.

Ransohoff RM, Perry VH. 2009. Microglial physiology: Unique stimuli, specialized responses. Annu Rev Immunol 27:119–145.

Rosenberg LJ, Teng YD, Wrathall JR. 1999. Effects of the sodium channel blocker tetrodotoxin on acute white matter pathology after experimental contusive spinal cord injury. J Neurosci 19:6122–6133.

Ryu J, Pyo H, Jou I, Joe E. 2000. Thrombin induces NO release from cultured rat microglia via protein kinase C, mitogen-activated protein kinase, and NF-kappa B. J Biol Chem 275:29955–29959.

Shigemoto-Mogami Y, Koizumi S, Tsuda M, Ohsawa K, Kohsaka S, Inoue K. 2001. Mechanisms underlying extracellular ATP-evoked interleukin-6 release in mouse microglial cell line, MG-5. J Neurochem 78:1339–1349.

Sontheimer H, Fernandez-Marques E, Ullrich N, Pappas CA, Waxman SG. 1994. Astrocyte Na+ channels are required for maintenance of Na+/K(+)-ATPase activity. J Neurosci 14:2464–2475.

Sun FY, Faden AI. 1995. Neuroprotective effects of 619C89, a use-dependent sodium channel blocker, in rat traumatic brain injury. Brain Res 673:133–140.

Teng YD, Wrathall JR. 1997. Local blockade of sodium channels by tetrodotoxin ameliorates tissue loss and long-term functional deficits resulting from experimental spinal cord injury. J Neurosci 17:4359–4366.

Tian DS, Dong Q, Pan DJ, He Y, Yu ZY, Xie MJ, Wang W. 2007. Attenuation of astrogliosis by suppressing of microglial proliferation with the cell cycle inhibitor olomoucine in rat spinal cord injury model. Brain Res 1154:206–214.

Trang T, Beggs S, Wan X, Salter MW. 2009. P2X4-receptor-mediated synthesis and release of brain-derived neurotrophic factor in microglia is dependent on calcium and p38-mitogen-activated protein kinase activation. J Neurosci 29:3518–3528.

Waetzig GH, Rosenstiel P, Arlt A, Till A, Brautigam K, Schafer H, Rose-John S, Seegert D, Schreiber S. 2005. Soluble tumor necrosis factor (TNF) receptor-1 induces apoptosis via reverse TNF signaling and autocrine transforming growth factor-beta1. FASEB J 19:91–93.

Wang X, Arcuino G, Takano T, Lin J, Peng WG, Wan P, Li P, Xu Q, Liu QS, Goldman SA, Nedergaard M. 2004. P2X7 receptor inhibition improves recovery after spinal cord injury. Nat Med 10:821–827.

Williams AJ, Tortella FC. 2002. Neuroprotective effects of the sodium channel blocker RS100642 and attenuation of ischemia-induced brain seizures in the rat. Brain Res 932:45–55.

Wilms H, Rosenstiel P, Sievers J, Deuschl G, Zecca L, Lucius R. 2003. Activation of microglia by human neuromelanin is NF-kappaB dependent and involves p38 mitogen-activated protein kinase: Implications for Parkinson's disease. FASEB J 17:500–502.

Xu JT, Xin WJ, Wei XH, Wu CY, Ge YX, Liu YL, Zang Y, Zhang T, Li YY, Liu XG. 2007. p38 activation in uninjured primary afferent neurons and in spinal microglia contributes to the development of neuropathic pain induced by selective motor fiber injury. Exp Neurol 204:355–365.

Yu FH, Catterall WA. 2003. Overview of the voltage-gated sodium channel family. Genome Biol 4:207.

Yune TY, Chang MJ, Kim SJ, Lee YB, Shin SW, Rhim H, Kim YC, Shin ML, Oh YJ, Han CT, Markelonis GJ, Oh TH. 2003. Increased production of tumor necrosis factor-alpha induces apoptosis after traumatic spinal cord injury in rats. J Neurotrauma 20:207–219.

Yune TY, Lee JY, Cui CM, Kim HC, Oh TH. 2009. Neuroprotective effect of Scutellaria baicalensis on spinal cord injury in rats. J Neurochem 110:1276–1287.

Yune TY, Lee JY, Jung GY, Kim SJ, Jiang MH, Kim YC, Oh YJ, Markelonis GJ, Oh TH. 2007. Minocycline alleviates death of oligodendrocytes by inhibiting pro-nerve growth factor production in microglia after spinal cord injury. J Neurosci 27:7751–7761.

Yune TY, Lee SM, Kim SJ, Park HK, Oh YJ, Kim YC, Markelonis GJ, Oh TH. 2004. Manganese superoxide dismutase induced by TNF-beta is regulated transcriptionally by NF-kappaB after spinal cord injury in rats. J Neurotrauma 21:1778–1794.

Zhang W, Wang T, Pei Z, Miller DS, Wu X, Block ML, Wilson B, Zhang W, Zhou Y, Hong JS, Zhang J. 2005. Aggregated alpha-synuclein activates microglia: A process leading to disease progression in Parkinson's disease. FASEB J 19:533–542.